JOURNAL OF SOLID STATE CHEMISTRY 34, 271–277 (1980)

Synthesis and Structural Study of the New Rare Earth Magnesium Borates $LnMgB_5O_{10}$ (Ln = La, . . . , Er)

BERNADETTE SAUBAT, MARCUS VLASSE, AND CLAUDE FOUASSIER

Laboratoire de Chimie du Solide du CNRS, Université de Bordeaux I, 351 cours de la Libération, 33405 Talence, Cedex, France

Received July 16, 1979; in revised form October 23, 1979

To obtain rare earth luminescent materials with weak concentration quenching, the B_2O_3-rich portion of the ternary diagram Ln_2O_3–MgO–B_2O_3 (Ln = rare earth) has been investigated. A ternary phase of composition $LnMgB_5O_{10}$ has been found for Ln = La, Ce, Pr, Nd, Sm, Eu, Gd, Tb, Dy, Ho, and Er. These compounds all crystallize in the monoclinic space group $P2_1/c$. The structure has been determined on a $LaMgB_5O_{10}$ crystal. A full-matrix least-squares refinement leads to R = 0.039. The structure can be described as being made of $(B_5O_{10}^{5-})_n$ two-dimensional layers linked together by the lanthanum and magnesium ions. The rare earth atom coordination polyhedra form isolated chains. These borates are isostructural with some rare earth cobalt borates.

Luminescent rare earth compounds with weak concentration quenching are of interest both as uv-excited phosphors (*1*, *2*) and as laser host structures for integrated optics (*3*). Most of them are rare earth phosphates (*4–6*). However, low-threshold room temperature continuous wave lasing has been recently reported in the boron-rich borate $NdAl_3(BO_3)_4$ (*7*). Compounds of the borate family seem therefore to be promising for high luminescent efficiency at high rare earth concentrations. Interactions between rare earth ions can only be reduced in phases with a weak Ln/O atomic ratio. Consequently, we have explored the B_2O_3-rich portion of the ternary diagram including the MgO and Ln_2O_3 oxides. A new rare earth borate family has been prepared with the composition $LnMgB_5O_{10}$.

Furthermore, in order to carefully study the influence of the host lattice and of the localization of the Ln atoms in the lattice on the luminescent properties, we have determined by X-ray diffraction the structure of one of these isostructural phases.

The Systems Ln_2O_3–MgO–B_2O_3

The oxides Ln_2O_3 (R.P., 99.99%), MgO (Cerac, 99.95%), and B_2O_3 (Cerac, 99.9%) were dissolved in concentrated nitric acid and the solution was evaporated to dryness. The resulting mixture was heated in an alumina crucible for 15 hr in air at 1000°C, and was then ground and annealed under the same conditions. Phase identification was carried out by powder X-ray diffraction. A ternary phase with composition $LnMgB_5O_{10}$ was found for Ln = La, Ce, Pr, Nd, Sm, Eu, Gd, Tb, Dy, Ho, Er. A portion of the La_2O_3–MgO–B_2O_3 diagram is shown in Fig. 1. Attempts to prepare $LnMgB_5O_{10}$ phases with smaller rare earths by modifying the preparation

0022-4596/80/120271-07$02.00/0

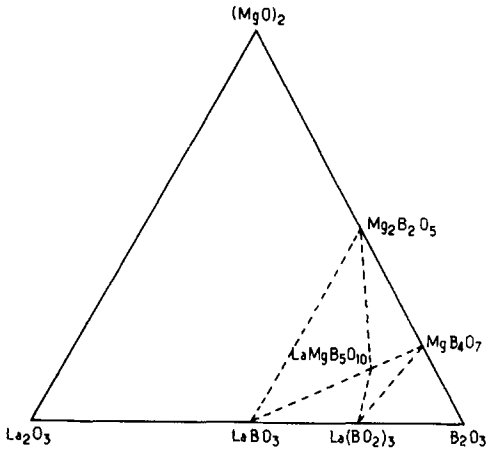

FIG. 1. Phase diagram for the boron-rich part of the La_2O_3–$(MgO)_2$–B_2O_3 system.

temperature were not successful. The variation of melting points indicates a decrease in the stability of the structure when the rare earth ion shrinks (Table I).

Crystallographic Data of $LnMgB_5O_{10}$ Phases

Single crystals of $LaMgB_5O_{10}$ have been obtained by melting a mixture of La_2O_3, MgO, and B_2O_3 at 1200°C and then cooling at a rate of 15°C per hour. MgO and B_2O_3 were in excess with respect to the stoichiometric amounts to compensate for volatilization losses.

TABLE I

MELTING POINTS FOR SOME $LnMgB_5O_{10}$ PHASES

	Ln			
	La	Nd	Eu	Er
t (°C)	1110	1075	1055	1020

Weissenberg and precession photographs characterize a monoclinic Laue symmetry $2/m$. The systematic absences, $h0l$, $l = 2n + 1$, and $0k0$, $k = 2n + 1$, are consistent with the space group $P2_1/c$. The cell dimensions obtained and refined from powder data are given in Table II. The cell contains four formula units ($\rho_{calc} = 3.923$ g cm^{-3} and $\rho_{exp} = 3.87 \pm 0.06$ g cm^{-3}).

The powder patterns of the other $LnMgB_5O_{10}$ phases show close similarities with that of the lanthanum phase and could be indexed on the basis of the same monoclinic unit cell with the space group $P2_1/c$. The unit-cell parameters are given in Table II.

Interplanar spacings of $LaMgB_5O_{10}$ are listed in Table III.

A single crystal of $LaMgB_5O_{10}$ in the form of a rectangular block 0.11 × 0.13 × 0.20 mm was mounted about the **b** axis. The intensities were measured on an Enraf–

TABLE II

UNIT-CELL DIMENSIONS FOR THE $LnMgB_5O_{10}$ PHASES

Ln	*a* (Å) ± 0.005	*b* (Å) ± 0.005	*c* (Å) ± 0.005	β (°)(±0.05°)	*V* (Å^3)
La	8.807	7.611	12.731	131.52	638.9314
Ce	8.798	7.612	12.653	131.50	634.6472
Pr	8.765	7.574	12.591	131.42	626.8005
Nd	8.755	7.549	12.569	131.40	623.1203
Sm	8.723	7.511	12.492	131.25	615.3482
Eu	8.710	7.511	12.500	131.22	615.1068
Gd	8.697	7.480	12.451	131.17	609.7217
Tb	8.683	7.455	12.394	131.04	605.1249
Dy	8.674	7.449	12.387	130.90	604.9523
Ho	8.654	7.424	12.366	130.82	601.2377
Er	8.611	7.400	12.317	130.66	595.3838

TABLE III

X-RAY DIFFRACTION DATA FOR $LaMgB_5O_{10}$[a]

I_{obs}	I_{calc}	d_{obs}	d_{calc}	$h\ k\ l$
100	100	6.60	6.59	1 0 0
72	75.4	6.32	6.34	1 0 $\bar{2}$
5	1.8	5.95	5.95	0 1 1; 0 1 $\bar{1}$
12	8.7	5.75	5.76	1 1 $\bar{1}$
18	20.2	4.86	4.87	1 1 $\bar{2}$
52	50.3	4.75	4.76	0 2 2; 0 2 $\bar{2}$
28	19.6	4.40	4.40	2 0 $\bar{2}$
88	89.4	3.81	3.81	2 1 $\bar{2}$; 0 2 0
35	33.2	3.53	3.53	0 2 1; 0 2 $\bar{1}$
37	32.5	3.49	3.49	2 1 $\bar{3}$; 1 2 $\bar{1}$
76	82.3	3.29	3.29	2 0 0; 1 2 0
63	43.5	3.26	3.26	1 2 $\bar{2}$
40	38.9	3.02	3.02	1 0 2; 2 1 0
34	25.6	2.969	2.974	0 2 2; 0 2 $\bar{2}$
84	66.8	2.921	2.928	2 1 $\bar{4}$
63	39.0	2.836	2.836 2.835	1 2 1 3 0 $\bar{2}$
22	17.1	2.792	2.797	1 2 $\bar{3}$
48	40.6	2.735	2.737 2.736	3 1 $\bar{3}$ 2 2 $\bar{3}$
33	29.5	2.656	2.656	3 1 $\bar{2}$
31	24.1	2.605	2.606	3 1 $\bar{4}$
30	27.9	2.492	2.492	2 2 0
26	13.7	2.479	2.481	2 1 1
38	37.8	2.432	2.438	0 2 3; 1 3 $\bar{1}$; 2 2 $\bar{4}$
13	12.5	2.409	2.411	3 1 $\bar{1}$
17	18.9	2.332	2.332	1 2 $\bar{4}$; 3 1 $\bar{5}$
10	7.8	2.274	2.274	0 1 4; 0 1 $\bar{4}$; 3 2 $\bar{2}$
20	18.2	2.160	2.161	1 3 $\bar{3}$; 2 2 1
5	4.3	2.153	2.151	2 3 $\bar{1}$
35	33.5	2.132	2.132	2 3 $\bar{3}$
40	45.2	2.110	2.111	3 0 $\bar{6}$; 4 1 4; 3 2 $\bar{1}$; 3 1 0
10	7.1	2.046	2.047	4 1 $\bar{5}$
38	36.2	2.032	2.038	3 1 $\bar{6}$; 4 0 $\bar{2}$
34	24.2	2.015	2.020	0 2 4
32	32.4	1.978	1.983	2 1 $\bar{6}$; 1 2 3; 0 3 3
31	30.3	1.959	1.959	4 1 $\bar{2}$
<1	3.5	1.954	1.955	1 2 $\bar{5}$
19	10.0	1.919	1.919	3 3 $\bar{3}$
20	13.7	1.902	1.906	4 1 $\bar{6}$
21	13.9	1.890	1.890	3 3 $\bar{2}$
34	25.7	1.867	1.866	0 4 1; 0 4 $\bar{1}$

[a] Cu$K\alpha_1$, λ = 1.5405 Å, using a Philips powder diffractometer.

Nonius CD3 three-circle automatic diffractometer with Mo$K\alpha$ radiation (λ = 0.70929 Å) and a pyrolytic graphite monochromator (002). A scintillation counter and a $\theta/2\theta$ multiple scanning technique with a scan rate of 10° (2θ) per minute were used. The background was taken at each end of the scan range for a time equal to the actual

TABLE IV

ATOMIC COORDINATES AND ANISOTROPIC TEMPERATURE FACTORS ($\times 10^{-5}$) FOR $LaMgB_5O_{10}$, WITH STANDARD DEVIATIONS IN PARENTHESES[a]

Atom	x	y	z	β_{11}	β_{22}	β_{33}	β_{13}	B (Å^2)
La	0.05141(3)	0.18847(4)	0.23410(2)	87(1)	65(6)	42(1)	40(1)	0.61(2)
Mg	0.5092(2)	0.4130(3)	0.1194(2)	227(21)	169(38)	109(10)	104(13)	1.56(21)
B(1)	0.6419(5)	0.0851(8)	0.2295(4)	126(48)	95(104)	61(23)	58(29)	0.88(51)
B(2)	0.9025(5)	0.3294(8)	0.3887(4)	118(46)	89(104)	56(22)	54(28)	0.82(50)
B(3)	0.2690(5)	0.0335(8)	0.0520(4)	108(47)	81(103)	52(23)	50(29)	0.65(49)
B(4)	0.8399(5)	0.0933(8)	0.4896(4)	117(48)	88(104)	56(23)	54(29)	0.82(49)
B(5)	0.4884(5)	0.3156(8)	0.4159(4)	144(47)	108(107)	69(23)	66(29)	1.00(50)
O(1)	0.7801(4)	0.2260(5)	0.2554(3)	167(34)	126(69)	80(16)	76(21)	1.16(30)
O(2)	0.6751(4)	0.0371(5)	0.3569(3)	195(35)	147(71)	93(17)	90(22)	1.36(31)
O(3)	0.3259(4)	0.4228(5)	0.3161(3)	216(36)	163(71)	104(17)	99(22)	1.51(30)
O(4)	0.4366(4)	0.1554(5)	0.1235(3)	181(35)	136(70)	87(17)	83(21)	1.26(30)
O(5)	0.7682(4)	0.4768(5)	0.3545(3)	232(37)	174(72)	111(18)	106(23)	1.61(32)
O(6)	0.0817(4)	0.3952(5)	0.4130(3)	130(33)	98(67)	62(16)	60(20)	0.91(29)
O(7)	0.9687(4)	0.2205(5)	0.5072(3)	166(34)	124(67)	79(16)	76(21)	1.15(29)
O(8)	0.6829(4)	0.3723(5)	0.4893(3)	208(36)	156(71)	100(18)	96(23)	1.45(32)
O(9)	0.4379(4)	0.1505(5)	0.4307(3)	216(36)	161(72)	103(18)	99(22)	1.50(32)
O(10)	0.8746(4)	0.4662(5)	0.1041(3)	253(38)	190(73)	121(18)	116(23)	1.76(33)

[a] The anisotropic temperature factor is: $\exp[-(h^2\beta_{11} + k^2\beta_{22} + l^2\beta_{33} + 2hk\beta_{12} + 2hl\beta_{13} + 2kl\beta_{23})]$, $\beta_{12} = \beta_{23} = 0$ for all atoms.

scan time. Three control reflections measured for every batch of 50 reflections showed a random fluctuation of about 4%. Three thousand and thirty-five independent reflections were measured ($2\theta_{max} = 90°$) with $I > 4\sigma(I)$ and were used in the refinement. These intensities were corrected for Lorentz and polarization effects, but not for absorption ($\mu_{Mo} = 69$ cm^{-1}, $\mu r_{max} = 0.7$).

Determination and Refinement of the Structure

A Patterson synthesis was used to determine the positions of the heavy lanthanum

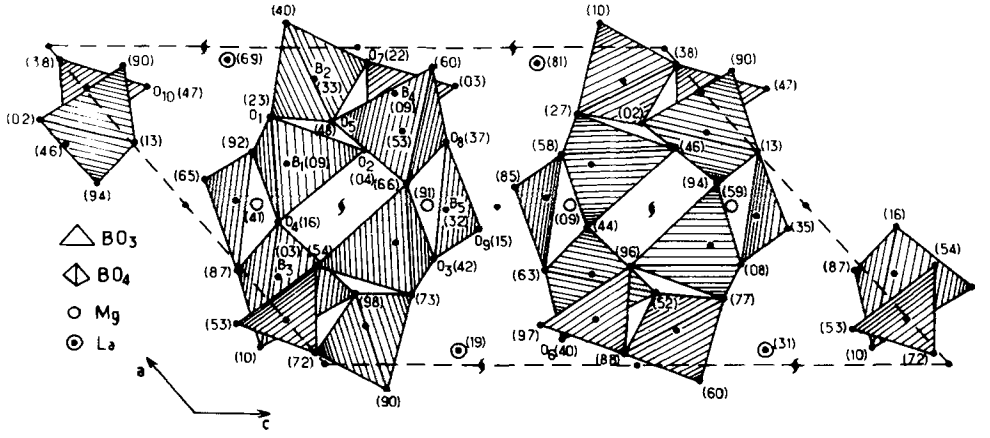

FIG. 2. Projection of the structure on the (010) plane.

TABLE V

INTERATOMIC DISTANCES (Å) FOR $LaMgB_5O_{10}$

B_1 tetrahedron	B_2 tetrahedron	B_3 tetrahedron
B_1–O_1 1.486(6)	B_2–O_1 1.495(6)	B_3–O_4 1.445(6)
B_1–O_2 1.490(6)	B_2–O_5 1.471(6)	B_3–O_5 1.493(6)
B_1–O_3 1.470(6)	B_2–O_6 1.480(6)	B_3–O_6 1.509(6)
B_1–O_4 1.464(6)	B_2–O_7 1.462(6)	B_3–O_8 1.502(6)
⟨B_1–O⟩ 1.478(6)	⟨B_2–O⟩ 1.477(6)	⟨B_3–O⟩ 1.487(6)
O_1–O_2 2.485(5)	O_1–O_5 2.328(5)	O_4–O_5 2.418(5)
O_1–O_3 2.429(5)	O_1–O_6 2.382(5)	O_4–O_6 2.448(5)
O_1–O_4 2.351(5)	O_1–O_7 2.445(5)	O_4–O_8 2.411(5)
O_2–O_3 2.363(5)	O_5–O_6 2.416(5)	O_5–O_6 2.503(5)
O_2–O_4 2.404(5)	O_5–O_7 2.481(5)	O_5–O_8 2.419(5)
O_3–O_4 2.443(5)	O_6–O_7 2.404(5)	O_6–O_8 2.358(5)
⟨O–O⟩ 2.412(5)	⟨O–O⟩ 2.409(5)	⟨O–O⟩ 2.426(5)
B_4 triangle	B_5 triangle	La–oxygen environment
B_4–O_2 1.376(6)	B_5–O_3 1.385(6)	La–O_1 2.593(3)
B_4–O_7 1.392(6)	B_5–O_8 1.368(6)	La–O_3 2.602(4)
B_4–O_{10} 1.354(6)	B_5–O_9 1.387(6)	La–O_6 2.633(3)
⟨B_4–O⟩ 1.374(6)	⟨B_5–O⟩ 1.378(6)	La–O_6 2.637(3)
O_2–O_7 2.395(5)	O_3–O_8 2.388(5)	La–O_7 2.562(3)
O_2–O_{10} 2.379(5)	O_3–O_9 2.343(5)	La–O_8 2.655(4)
O_7–O_{10} 2.363(5)	O_8–O_9 2.435(5)	La–O_9 2.577(4)
⟨O–O⟩ 2.379(5)	⟨O–O⟩ 2.389(5)	La–O_{10} 2.493(4)
Mg–oxygen environment	Metal–Metal	La–O_{10} 2.398(4)
Mg–O_1 2.289(4)	La–La 3.994(5)	La–O_5 2.961(4)
Mg–O_2 2.066(4)	La–Mg 3.833(2)	⟨La–O⟩ 2.591(4)
Mg–O_4 2.074(4)	Mg–Mg 3.220(4)	
Mg–O_5 2.312(4)	La–Mg 3.644(3)	
Mg–O_9 2.097(4)		
Mg–O_9 2.070(4)		
⟨Mg–O⟩ 2.151(4)		

atoms. The boron and oxygen atoms were located in a difference synthesis at an intermediate stage of the refinement. Full-matrix least-squares refinement (*8*) with anisotropic temperature factors reduced $R = \Sigma||F_o|F_c||/\Sigma|F_o|$ to 0.039, based on a data-to-parameter ratio of 20 to 1. A final $(F_o - F_C)$ synthesis confirmed the proposed solution.

$\Sigma W(|F_o - F_c|)^2$ was minimized with W taken as unity for all reflections. The overall scale factor had the final value of 7.68 ($F_o = kF_c$). The form factors for La, Mg, B, and O were taken from McMaster *et al.* (*9*), with real and imaginary anomalous dispersion terms given by Cromer (*10*).

The final atomic and thermal parameters are given in Table IV. Table V contains the interatomic distances and angles.

Description and Discussion

A projection of the structure on the (010) plane is given in Fig. 2. A comparison with the structure of $SmCo(BO_2)_5$ (*11*) shows that the two structures are isostructural with La in the place of Sm and Mg replacing

Co, similarly with $LaCo(BO_2)_5$ and $HoCo(BO_2)_5$ (*12*, *13*).

The structure of $LaMgB_5O_{10}$ can be easily described as being made of infinite two-dimensional boron–oxygen layers, parallel to the (102) plane, linked together by the lanthanum and magnesium atoms. Each of these infinite slabs consists of groups of three BO_4 tetrahedra and two BO_3 triangles sharing corners, giving a boron–oxygen anionic complex $[B_5O_{10}]_n^{5-}$ (Fig. 2). The boron atoms B_1, B_2, and B_3 are found in a tetrahedral coordination, while B_4 and B_5 have triangular surroundings.

The lanthanum atom has 10-fold coordination with eight normal distances, one shorter distance, and one longer distance. As can be seen in Fig. 3, it is surrounded by three boron triangles and three boron tetrahedra with which the lanthanum atom shares either edges or corners. The only significant O–O distances surrounding the La atom are those belonging to the boron polyhedra ($d_{O-O} < 2.55$ Å).

Similarly, the Mg atom has a six-fold coordination with four normal and two slightly longer distances. It shares oxygen atoms with three BO_4 and two BO_3 groups (Fig. 4). It can also be seen in Figs. 2 and 4 that the two neighboring Mg atoms form a sort of dimer (Mg–Mg = 3.220 Å), sharing the two oxygen atoms O_9.

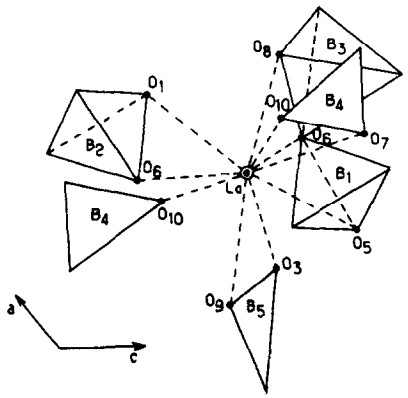

FIG. 3. Lanthanum atom environment.

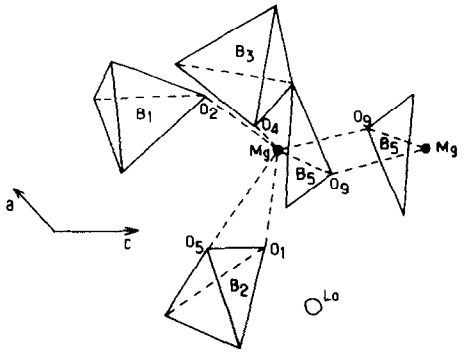

FIG. 4. Environment of the magnesium atom.

The mean boron–oxygen distances are 1.478, 1.477, and 1.487 Å for the three BO_4 units and 1.374 and 1.378 Å for the BO_3 groups. This result compares well with the corresponding mean bond distances given by Martinez-Ripoll *et al.* (*14*) (1.46 Å in BO_4 and 1.37 Å in BO_3).

The average La–O and Mg–O distances are, respectively, 2.591 and 2.151 Å, a result close to the sum of the effective ionic radii which is an indication of rather ionic bonding between La^{3+}, Mg^{2+}, and the complex unit $[B_5O_{10}]^{5-}$. Of course the bonding in the boron polyhedra is predominantly covalent, as witnessed by the short B–O and O–O distances in these groupings.

The lanthanum atoms form infinite zigzag chains along the **b** axis. The La–La distances inside these chains are 3.994 Å, while those between the chains are 6.430 Å. These distances certainly show that *Ln–Ln* interactions in this type of structure can only exist inside each chain. The La–Mg distance is 3.644 Å.

We can then conclude that the existence of well-isolated *Ln* chains in a highly covalent matrix could be favorable to relatively low concentration quenching. The luminescent properties will be described elsewhere.

References

1. Y. TSUJIMOTO, Y. FUKUDA, AND FUKAI, *J. Electrochem. Soc.* **124**(4), 553 (1977).

2. J. FAVA, A. PERRIN, J. C. BOURCET, R. SALMON, C. PARENT, AND G. LE FLEM, *J. Lumin.* **18/19**, 389 (1979).
3. S. R. CHINN, H. Y. P. HONG, AND J. W. PIERCE, *Laser Focus* **12**(5), 64 (1976).
4. H. G. DANIELMEYER AND H. P. WEBER, *IEEE J. Quantum Electron.* **8**(10), 805 (1972).
5. K. OTSUKA, T. YAMADA, M. SARUWATARI, AND T. KIMURA, *IEEE J. Quantum Electron.* **11**, 330 (1975).
6. J. C. MICHEL, D. MORIN, AND F. AUZEL, *C.R. Acad. Sci. Paris* **281**, 445 (1975).
7. S. R. CHINN AND H. Y. P. HONG, *Opt. Commun.* **15**, 345 (1975).
8. W. R. BUSING, K. O. MARTIN, AND H. A. LEVY, ORFLS Report ORNL-TM-305, Oak Ridge National Laboratory, Oak Ridge, Tenn. (1962).
9. W. H. MCMASTER, N. KERR DEL GRANDE, J. H. MOLLET, AND J. H. HUBBEL, "Compilation of X-Ray Cross-Sections," UCRL-50174, Sect. II, Rev. 1, Nat. Bur. Stand., Washington, D.C. (1969).
10. D. T. CROMER, *Acta Crystallogr. Sect. B* **18**, 17 (1965).
11. G. K. ABDULLAEV, K. S. MAMEDOV, AND G. G. DZHAFAROV, *Sov. Phys. Crystallogr.* **19**(4), 457 (1975).
12. G. K. ABDULLAEV, K. S. MAMEDOV, AND G. G. DZHAFAROV, *Zh. Strukt. Khim.* **16**(1), 71 (1975).
13. G. K. ABDULLAEV, K. S. MAMEDOV, I. R. AMIRASLANOV, G. G. DZHAFAROV, D. A. ALIEV, AND B. T. USUBALLIEV, *Zh. Neorg. Khim.* **23**(9), 2332 (1978).
14. M. MARTINEZ-RIPOLL, S. MARTINEZ-CARRERA, AND S. GARCIA-BLANCO, *Acta Crystallogr. Sect. B* **27**, 672 (1971).